FPMC2022-89984

A MULTIMODAL CLIMBING-SWIMMING SOFT ROBOTIC LAMPREY

James Gallentine* Eric J. Barth Kevin Galloway

Laboratory for the Design and Control of Energetic Systems
Mechanical Engineering
Vanderbilt University
Nashville, Tennessee 37235

Brian Van Stratum
Jonathan Clark
Kourosh Shoele
STRIDe / CTML
Florida State University
Tallahassee, Florida 32310

ABSTRACT

Here, we present a multimodal, lamprey-inspired, 3D printed soft fluidic robot/actuator based on an antagonistic pneunet architecture. The Pacific Lamprey is a unique fish which is able to climb wetted vertical surfaces using its suction-cup mouth and snake-like morphology. The continuum structure of these fish lends itself to soft robots, given their ability to form continuous bends. Additionally, the high gravimetric and volumetric power density attainable by soft actuators make them good candidates for climbing robots. Fluidic soft robots are often limited in the forces they can exert due to limitations on their actuation pressure. This actuator is able to operate at relatively high pressures (for soft robots) of 756 kPa (95 psig) with a -3 dB bandwidth of 2.23 Hz to climb at rates exceeding 18 cm/s. The robot is capable of progression on a vertical surface using a compliant microspine attachment as the functional equivalent of the lamprey's more complex suction-cup mouth. The paper also presents the details of the 3D-printed manufacturing of this actuator/robot.

INTRODUCTION

The Pacific Lamprey is an adept rock climber, able to ascend waterfalls to swim further upstream [1]. These fish create powerful contractions with their outwardly unadorned, snakelike morphology to dynamically leap upward and attach to rocks with their suction-cup mouths. Creatures with serpentine body



FIGURE 1. PNEUMATIC CLIMBING ROBOT INSPIRED BY THE PACIFIC LAMPREY. THE SOFT ACTUATOR CONSISTS OF TWO 135 MM ANTAGONISTIC PNEUNETS

shapes, such as snakes, are capable of a large variety of locomotion methods including crawling, swimming, climbing, and even gliding. Moreover, continuum physiology such as elephant trunks and octopus arms demonstrate a massive range of capabilities in both strength and dexterity.

Bio-inspired, legged wall-climbing robots designed using reduced-order dynamic models have achieved speed, agility, efficiency and are robust to disturbances [2–4]. By coordinating the system's energy exchange between the kinetic and potential energies, these dynamic climbing robots achieve good climbing performance. Recently a dynamic lamprey-inspired gait was demonstrated on a segmented robot in hardware and simulation [5].

Fluid powered soft robots allow a unique option for the

^{*}Address all correspondence to this author.

adaptation of serpentine actuation. Soft robots have demonstrated a wide variety of locomotion methods [6]. Due to their elastic construction, they are able to achieve continuous curves and high gravimetric and volumetric power densities, relative to rigid-link bio-inspired robots. Soft robots are a natural direction for the development of mechanical systems which are able to capitalize on the capabilities of biological continuum physiologies. Morover, when combined with the capabilities of 3D printing, pneumatic and hydraulic actuators can be created which are capable of exhibiting complex motions without complicated manufacturing or technical casting steps [7] [8]. Generally, soft robots are designed to actuate with relatively low pressures under 450 kPa [9]. Many even prioritize low-operation pressure [10], limiting the forces which they are able to apply.

As a demonstration of the potential for power-dense soft fluidic robots, a multimodal robot inspired by the Pacific Lamprey is presented which is capable of operating at relatively high pressures and bandwidths. The success of Pacific Lamprey inspiration has been previously demonstrated in segmented robots [5]. Climbing robots have been demonstrated which use fluidic actuators in a rigid frame [11]. Here, a climbing robot is presented which is composed primarily of soft materials. Climbing at relatively high speeds is demonstrated using a continuum body shape via two investigated gaits. The resultant robot is composed of relatively few parts, the body of which is exceedingly durable.

1 Methods

The actuator body of the lamprey robot was 3D printed out of Ninjaflex (Ninjatek) thermoplastic polyurethane (TPU) filament with a shore hardness of 85A. This soft material allowed for flexible and air-tight prints. Printing was done on a Taz6 3D printer (Lulzbot) modified with a Dual Flexion extruder (Diabase Engineering) and Klipper firmware. To achieve air-tight prints capable of holding over 756 kPa, printed walls were made with 5 layers of 0.4 mm extrusions and 0.3 mm layer heights. All printing was over-extruded at 115 %. The actuator design was refined using the guidance of prior works [12] and empirical refinement.

The final actuator body consisted of two segments of 135 mm long, bidirectional, antagonistic, pneunet [10] actuators as shown in Fig. 1. Each of the four resultant chambers could be independently pressurized to control both total bending moment and relative stiffness of the two segments. The internal geometry of the pneunet actuator can be seen in Fig. 2. For the climbing gaits investigated, the four chambers were externally conjoined into two sets of two to form a planar actuator with one degree of freedom. The central axis of the actuator was created with a thicker wall to act as a strain-limiting layer to the four chambers. Fig. 5 shows the fully-actuated robot with conjoined chambers.

Climbing surface attachment was achieved using compliant microspine arrays mounted to the head of the robot [13]. Standins for the head and mouth of a biological lamprey, these passive

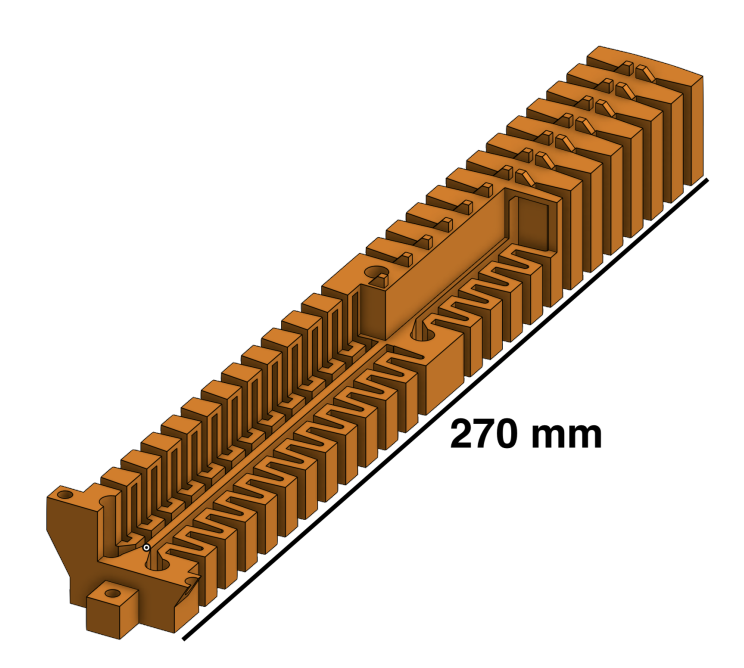


FIGURE 2. SECTION VIEW SHOWING INTERNAL GEOMETRY OF ACTUATOR CHAMBERS. CHAMBERS WERE CONJOINED TO ENABLE GAITS DISCUSSED

mechanisms allowed for consistent, unidirectional attachment to a climbing surface by exploiting asperities in the surface. As the goal was to evaluate the lamprey body morphology for climbing, microspines were chosen as a simple, passive option for attachment implementation. Each microspine (Fig. 3) was created using a fishhook embedded in rigid Task 9 urethane (Smooth-On) co-molded with soft ReoFlex 20A urethane rubber (Smooth-On). The compliant nature of the mounting maintained contact between the fishhook and climbing surface, which thereby increased the chance of successfully catching a surface asperity.

The microspines were connected in groups using 3D printed ABS mounts. Two layouts of microspine arrays were investigated as shown in Fig. 4. Each arrangement contained a total of 10 microspines. The first, consisted of two microspine arrays mounted to the sides of the robot, up to 36mm from the central axis. This allowed for a gait which included pendulum aspects, switching the connection point between the two arrays. Due to instability caused by the two-array climbing motion, the robot's attachment head was modified with kickstands to prevent the robot from twisting off the wall. The second attachment layout was comprised of a single microspine array located along the central axis of the robot, more similar to the mouth placement of a biological lamprey. To encourage climbing when using the single-array attachment configuration, a 100 g mass was connected to the tail of the robot, shifting the center of mass lower on its body.

Pressurization of the pneunet actuators was acheived using a

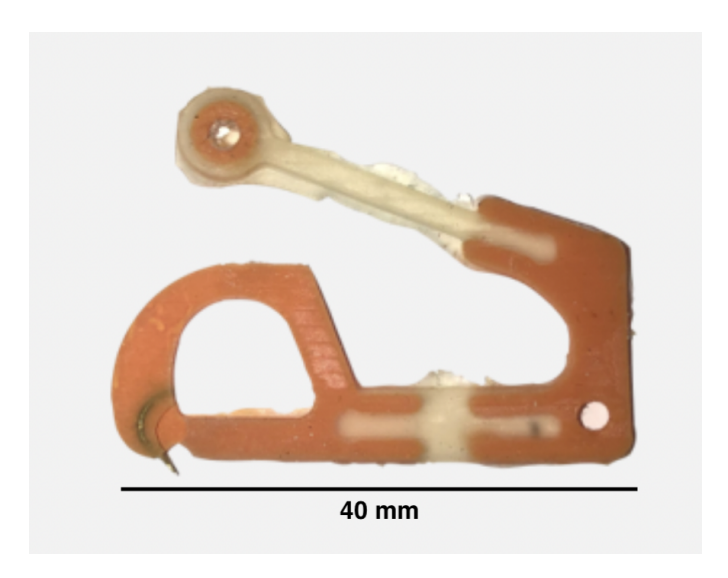


FIGURE 3. EXAMPLE OF MICROSPINE USED TO ATTACH ROBOT TO CLIMBING SURFACE. DARK-ORANGE: TASK-9 URETHANE, TRANSLUSCENT: REOFLEX 20 SOFT URETHANE. COMPLIANT NATURE MAINTAINS CONTACT BETWEEN HOOK AND SURFACE

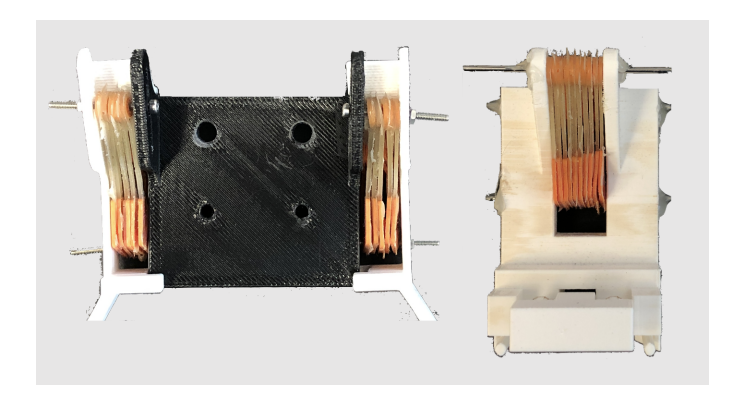


FIGURE 4. TWO ATTACHMENT CONFIGURATIONS CONSIDERED. LEFT: TWO OUTBOARD ATTACHMENT POINTS, RIGHT: SINGLE CENTRAL ATTACHMENT POINT

MPYE-5-M5-010-B proportional spool valve (Festo) and quantified with SDE-16-10V/20mA pressure transducers (Festo) such that the commanded pressure difference between the two chambers in each segment was controlled by a PID loop. Physical attachment of pressure lines to the actuator body was achieved via barbed fittings (McMaster-Carr) and push-to-connect fittings (SMC Pneumatics).

For the purposes of climbing, the actuator layout enabled two gaits which were tested. The first, an 'S' shaped bend mimicked a biological lamprey's motion more closely than the second. Hereafter referred to as the S-gait, it involved pressurizing the chambers diagonal to each other, creating opposite curvature

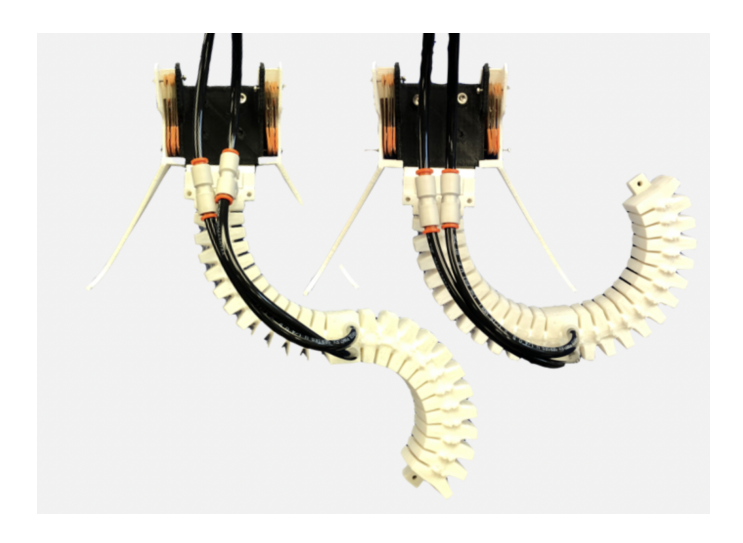


FIGURE 5. LEFT: FULLY CONTRACTED S-GAIT, RIGHT: FULLY CONTRACTED C-GAIT

in the segments distal and proximal to the head. The second, a C-gait, formed a bend by pressurizing the chambers on the same side of the actuator, creating bends with matching curvatures in each segment (Figure 5). Fig. 9 shows instants from a complete stride cycle in the C-gait, clarifying the actuation of the robot.

The robot was actuated using square waves between $0.15~\mathrm{Hz}$ and $4.28~\mathrm{Hz}$ to examine its climbing performance at a variety of actuation frequencies. The commanded pressure difference for each actuation cycle was $620~\mathrm{kPa}$.

During climbing, a stride was considered to be a complete square wave producing two steps. Visually, a stride consists of two complementary pressurizations, one bending the actuator body rightward, and one bending the actuator body leftward.

To aid in robust climbing and performance measurement, a climbing surface was created with burlap fabric stretched across a flat sheet of cork board. This surface was then angled to 30° off vertical. A tape measure was fixed to the board to aid in climbing measurement and verify camera tracking results. The lamprey was initially positioned on top of this surface near the bottom of the board for each test. While climbing was observed on a vertical surface, the angle of the board was chosen as a compromise to aid in attachment consistency. The effect of angle on climbing performance was not quantified for this work.

Measurements of climbing performance were taken at 30 frames per second (FPS) via a camera fixed 2 m from and parallel to the climbing surface. Digital video of the lamprey was both manually marked and processed using Tracker software [14] and automatically marked and processed using DeepLabCut software [15, 16]. Measurements were extracted from digital video pixel data and observed to be reproducible to sub millimeter precision. With DeepLabCut, a Resnet-50 neural network was trained on 179 manually labeled images of the lamprey climbing

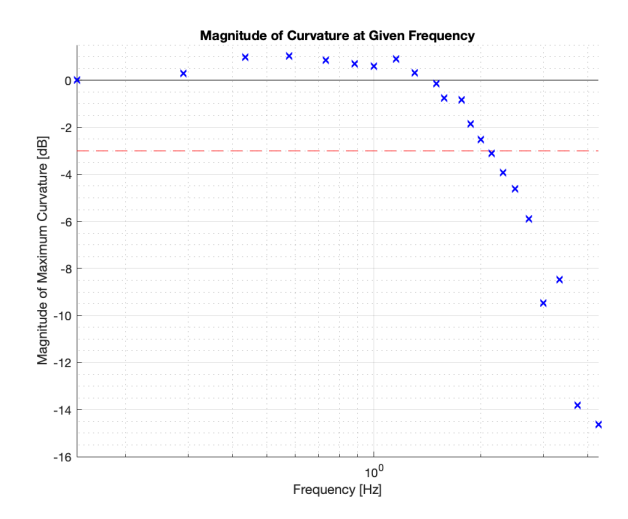


FIGURE 6. SEGMENT CURVATURE VS ACTUATION FREQUENCY.

for 40,000 training iterations to allow the software to track points along the body of the robot. This software uses machine learning to allow for markerless pose estimation and position tracking. The training set included images of both climbing gaits and attachment modes.

For both gaits and each frequency investigated, the distance traveled by the robot over a series of consecutive actuation and attachment cycles was measured for cases where attachment was maintained. This was used to calculate an average distance climbed per actuation cycle and speed of climbing for a given gait and actuation frequency.

Swimming and swim-climb transition of the lamprey robot was demonstrated by attaching a plastic tail fin. However this swimming performance has not been quantified in this paper.

Results

The 3D printed actuator body of the lamprey, consisting of two 135mm sections, weighed 0.220 kg. It was demonstrated to be capable of rapid actuation at relatively high pressures in excess of 756 kPa. Using DeepLabCut software to analyze recorded video, the actuator was found to have a -3 dB bandwidth of 2.23 Hz as shown in Fig. 6. The magnitude of curvature was calculated as the percent of curvature relative to the maximum steady-state curvature converted to decibels. When a single segment chamber was actuated to a constant pressure of 756 kPa, the segment of the actuator was deflected 105° from its central position. Additionally, at this pressure, the actuator body was able to contract in both gait configurations with a force of 3.98 kg hung vertically downward and fixed head.

Actuators were able to be deformed heavily without incurring damage or loss of functionality. Failure of the actuators was

uncommon, however, was possible at sufficiently high pressures. Failure occurred in 2 out of 7 actuators tested. Failure always occurred between print layers. An actuator which developed a small hole would continue to function with most of its operational range retained. Holes and splits between seams would continue to spread along the seam, gradually decreasing actuator performance. Therefore, these actuators exhibited a graceful degradation when material failure did occur.

Climbing performance was evaluated for each gait and attachment configuration at a range of frequencies as shown in Fig. 7. Maximum vertical displacement per stride was observed for the C-gait at 2.5 Hz. In the S-gaits, maximum vertical displacement per stride was seen at a lower frequency of 1.76 Hz. Maximum vertical climbing speed did not necessarily coincide with maximum per-stride displacement, as seen in Fig. 8. Climbing speeds increased roughly linearly at low frequencies, however, as the frequency increased, the per-stride displacement decreased with total actuator curvature, limiting the climb rate.

Figure 9 shows the results of a gait analysis similar to that done for geckos and cockroaches [17]. This analysis compares the resulting climbing performance, Right spine-Left spine attachment phasing, and corresponding video frames. This detail analysis was conducted for the 3.33 Hz C bend actuation case which is among the faster experiments. The analysis includes clipping the lamprey robot displacement data generated with the Tracker software. Data was binned according to the percent of stride and mean and standard deviation was computed for each group. Solid and dashed lines in Fig. 9 show the mean and standard deviation from this analysis. The lamprey robot climbs in this case with an typical stride length of 6.0 cm (SD 1.9 N 10). Since the data is for climbing at a tail beat frequency of 3.33Hz the resulting climbing speed is 18.0 cm/s with peaks observed over 26.3 cm/s.

Differences in relative stability of climbing performance and consistency were observed for each gait and configuration. For the two-array configuration, climbing in the S-gait was slower, yet attached more consistently than the C-gait. The one-array S-gait was the most consistent at attaching and climbing, however, the one-array C-gait was unable to attach and did not exhibit climbing behavior.

In the single-point attachment configuration, climbing was achieved solely using a flight phase in the stride where "flight phase" indicates that all points of attachment to the wall were completely unweighted. As achieving a flight phase is dependent on a vertical displacement of the robot center of mass, climbing was not observed without additional mass attached to the tail of the lamprey. With the added inertia and distally-shifted center of gravity, a flight phase was achieved and the robot was able to make vertical progress.

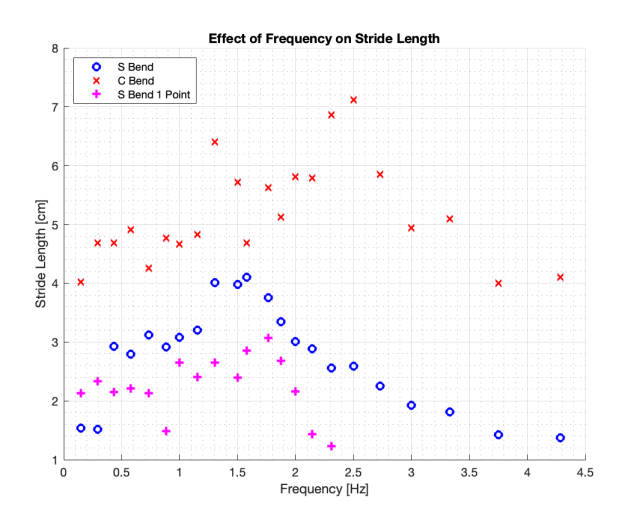


FIGURE 7. AVERAGE VERTICAL DISPLACEMENT PER STRIDE AT DIFFERENT FREQUENCIES

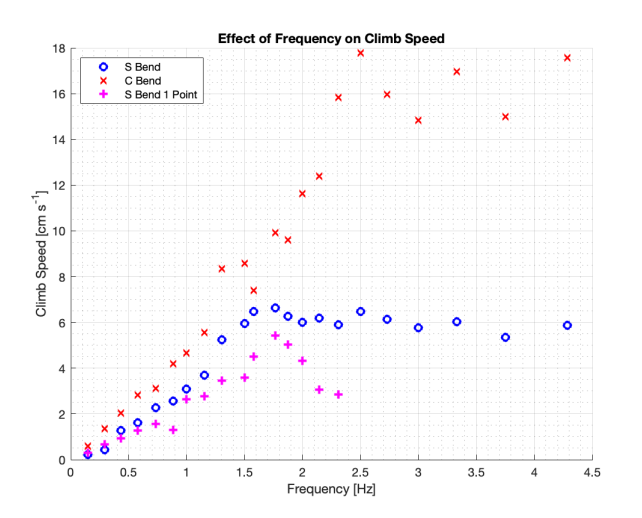
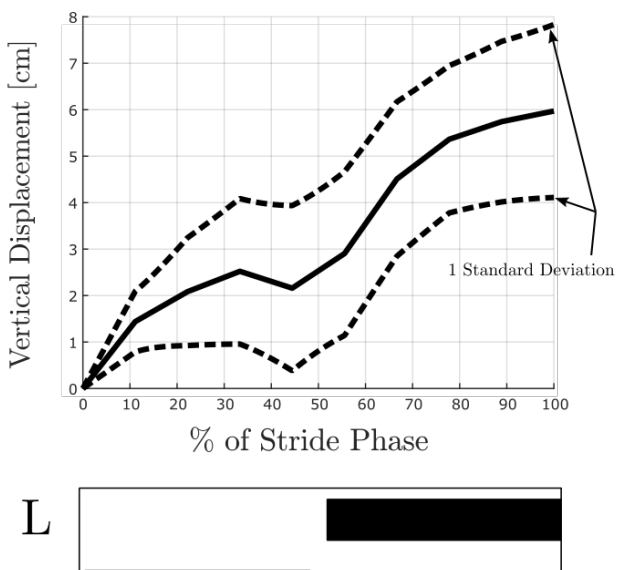


FIGURE 8. AVERAGE VERTICAL SPEED FOR ACTUATION AT DIFFERENT FREQUENCIES.

2 Discussion

3D printing soft actuators opens up the potential for programming complex motions directly into the physical structure of the actuator. This allows actuators to be quickly produced for unique applications. These actuators can be designed to operate at relatively high bandwidths and pressures. The advantages afforded by these new manufacturing techniques allow for the use of fluid power to an increasing range of applications. They allow fluidic actuators to be produced capable of complex motions in relatively compact and lightweight packages.

Printing of the lamprey robot was accomplished using 85A



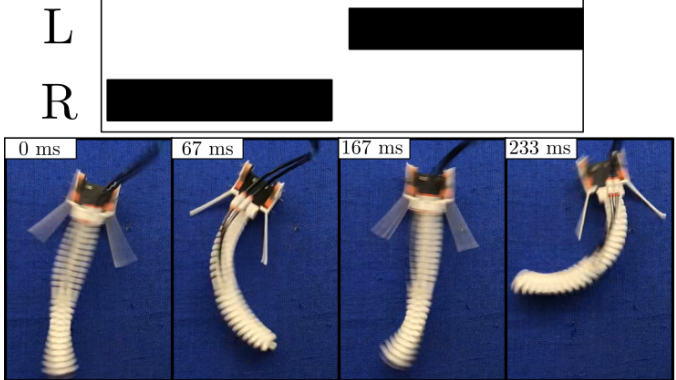


FIGURE 9. PHASING OF ATTACHMENT AND DISPLACEMENT OF LAMPREY INSPIRED SOFT ROBOT HEAD.

shore hardness TPU filament. There are many other filaments are available for 3D printing with different properties. Filaments are available as soft as 60A and slightly harder at 95A. Softer filaments may be good for actuators which operate with lower pressures or which require a higher degree of flexion. Harder filaments may be capable of higher actuation pressures, increased operational bandwidth, and increased force output. Additionally, actuators could be printed with multiple materials of different Shore hardnesses to further customize the behavior of the robot.

Climbing performance was evaluated using two attachment strategies, each of which highlighted a different modality of climbing. The dual-point attachment primarily climbed by driving an attachment point vertically using both the actuator's contraction and a pendulum motion resulting from a horizontal shift in the actuator's center of gravity. The single-point attachment climbed solely via a flight phase generated by shifting its center of gravity vertically. The center of gravity was shifted distally to increase its displacement using a mass on the robot's tail. Especially at low frequencies, it is likely that a flight phase could be introduced to the two-point attachment, increasing its climb rate.

A target of this research is a soft robot capable of multimodal locomotion by swimming, crawling, and climbing. Swimming was demonstrated by the design presented, however, it was not quantified for this paper.

ACKNOWLEDGMENT

This work was funded by the National Science Foundation Expanding Frontiers in Research and Innovation Program, grant number 1935278.

REFERENCES

- [1] Kemp, P., Tsuzaki, T., and Moser, M., 2009. "Linking behaviour and performance: intermittent locomotion in a climbing fish". *Journal of Zoology*, **277**(2), pp. 171–178.
- [2] Dickson, J., and Clark, J., 2012. "The effect of sprawl angle and wall inclination on a bipedal, dynamic climbing platform". In *Adaptive Mobile Robotics*. World Scientific, pp. 459–466.
- [3] Lynch, G. A., Clark, J. E., Lin, P.-C., and Koditschek, D. E., 2012. "A bioinspired dynamical vertical climbing robot". *The International Journal of Robotics Research*, *31*(8), pp. 974–996.
- [4] Provancher, W. R., Jensen-Segal, S. I., and Fehlberg, M. A., 2010. "Rocr: An energy-efficient dynamic wall-climbing robot". *IEEE/ASME Transactions on Mechatronics*, 16(5), pp. 897–906.
- [5] Van Stratum, B., Shoele, K., and Clark, J., 2021. Reduced order model of lamprey-inspired wall climbing. https://www.dynamicwalking2021.org/episode-1-biomechanics. Ep: 1.
- [6] Calisti, M., Picardi, G., and Laschi, C., 2017. "Fundamentals of soft robot locomotion". *Journal of the Royal Society Interface*, 14(130), May, p. 20170101. Place: London Publisher: Royal Soc WOS:000402534200022.
- [7] Marchese, A. D., Katzschmann, R. K., and Rus, D., 2015. "A Recipe for Soft Fluidic Elastomer Robots". *Soft Robotics*, 2(1), Mar., pp. 7–25. Place: New Rochelle Publisher: Mary Ann Liebert, Inc WOS:000364570300003.
- [8] Gul, J. Z., Sajid, M., Rehman, M. M., Siddiqui, G. U., Shah, I., Kim, K.-H., Lee, J.-W., and Choi, K. H., 2018. "3D printing for soft robotics - a review". *Science and Technology of Advanced Materials*, 19(1), Mar., pp. 243–262. Place: Abingdon Publisher: Taylor & Francis Ltd WOS:000443891300001.
- [9] Yap, H. K., Ng, H. Y., and Yeow, C.-H., 2016. "High-Force Soft Printable Pneumatics for Soft Robotic Applications". *Soft Robotics*, 3(3), Sept., pp. 144–158. Publisher: Mary Ann Liebert, Inc., publishers.
- [10] Mosadegh, B., Polygerinos, P., Keplinger, C., Wennstedt, S., Shepherd, R. F., Gupta, U., Shim, J., Bertoldi, K.,

- Walsh, C. J., and Whitesides, G. M., 2014. "Pneumatic Networks for Soft Robotics that Actuate Rapidly". *Advanced Functional Materials*, 24(15), pp. 2163–2170.
- [11] Bryant, M., Fitzgerald, J., Miller, S., Saltzman, J., Kim, S., Lin, Y., and Garcia, E., 2014. "Climbing robot actuated by meso-hydraulic artificial muscles". In Active and Passive Smart Structures and Integrated Systems 2014, Vol. 9057, SPIE, pp. 148–159.
- [12] Gu, G., Wang, D., Ge, L., and Zhu, X., 2021. "Analytical Modeling and Design of Generalized Pneu-Net Soft Actuators with Three-Dimensional Deformations". *Soft Robotics*, 8(4), Aug., pp. 462–477. Publisher: Mary Ann Liebert, Inc., publishers.
- [13] Asbeck, A. T., Kim, S., Cutkosky, M. R., Provancher, W. R., and Lanzetta, M., 2006. "Scaling hard vertical surfaces with compliant microspine arrays". *The International Journal of Robotics Research*, 25(12), pp. 1165–1179.
- [14] Open Source Physics. Tracker video analysis and modeling tool.
- [15] Mathis, A., Mamidanna, P., Cury, K. M., Abe, T., Murthy, V. N., Mathis, M. W., and Bethge, M., 2018. "DeepLab-Cut: markerless pose estimation of user-defined body parts with deep learning". *Nature Neuroscience*, 21(9), Sept., pp. 1281–1289. Number: 9 Publisher: Nature Publishing Group.
- [16] Nath, T., Mathis, A., Chen, A. C., Patel, A., Bethge, M., and Mathis, M. W., 2019. "Using DeepLabCut for 3D markerless pose estimation across species and behaviors". *Nature Protocols*, *14*(7), July, pp. 2152–2176. Number: 7 Publisher: Nature Publishing Group.
- [17] Goldman, D. I., Chen, T. S., Dudek, D. M., and Full, R. J., 2006. "Dynamics of rapid vertical climbing in cockroaches reveals a template". *Journal of Experimental Biol*ogy, 209(15), pp. 2990–3000.